






Article

Hierarchical Control of Power Distribution in the Hybrid Energy Storage System of an Ultrafast Charging Station for Electric Vehicles

Alexandra Blanch-Fortuna ¹, David Zambrano-Prada ¹, Oswaldo López-Santos ¹, Abdelali El Aroudi ¹, Luis Vázquez-Seisdedos ² and Luis Martínez-Salamero ^{1,*}

- ¹ Group of Automatic Control and Industrial Electronics (GAEI), Department of Electrical, Electronic and Automatic Control Engineering, School of Electrical and Computer Engineering, Rovira i Virgili University, Campus Sescelades, 43007 Tarragona, Spain; alexandra.blanch@urv.cat (A.B.-F.); davidalejandro.zambrano@urv.cat (D.Z.-P.); oswaldo.lopez@urv.cat (O.L.-S.); abdelali.elaroudi@urv.cat (A.E.A.)
- ² Electrotechnics Teaching Unit, Department of Forestry Engineering and Management, School of Forestry Engineering and Natural Resources, Technical University of Madrid, 28040 Madrid, Spain; luis.vazquez@upm.es
- * Correspondence: luis.martinez@urv.cat

Abstract: This paper presents a two-level hierarchical control method for the power distribution between the hybrid energy storage system (HESS) and the main dc bus of a microgrid for ultrafast charging of electric vehicles (EVs). The HESS is composed of a supercapacitor and a battery and is an essential part to fulfill the charging demand of EVs in a microgrid made up of a 220 V_{RMS} ac bus, two dc buses of 600 V and 1500 V, respectively, and four charging points. A state machine defines the four operating modes of the HESS and establishes the conditions for the corresponding transitions among them, namely, charging the battery and the supercapacitor from the bus, injecting the current from the HESS into the 1500 V dc bus to ensure the power balance in the microgrid, regulating the bus voltage, and establishing the disconnection mode. The primary level of the control system regulates the current and voltage of the battery, supercapacitor, and dc bus, while the secondary level establishes the operating mode of the HESS and provides the appropriate references to the primary level. In the primary level, sliding mode control (SMC) is used in both the battery and supercapacitor in the inner loop of a cascade control that implements the standard constant current–constant voltage (CC-CV) charging protocol. In the same level, linear control is applied in the CV phase of the protocol and for bus voltage regulation or the current injection into the bus. PSIM simulations of the operating modes and their corresponding transitions verify the theoretical predictions.

Keywords: ultrafast charging station; hybrid energy storage system; power sharing; sliding mode control



Citation: Blanch-Fortuna, A.; Zambrano-Prada, D.; López-Santos, O.; Aroudi, A.E.; Vázquez-Seisdedos, L.; Martínez-Salamero, L. Hierarchical Control of Power Distribution in the Hybrid Energy Storage System of an Ultrafast Charging Station for Electric Vehicles. *Energies* **2024**, *17*, 1393. <https://doi.org/10.3390/en17061393>

Academic Editor: Piedad Garrido Picazo

Received: 30 January 2024

Revised: 6 March 2024

Accepted: 12 March 2024

Published: 14 March 2024



Copyright: © 2024 by the authors. Licensee MDPI, Basel, Switzerland. This article is an open access article distributed under the terms and conditions of the Creative Commons Attribution (CC BY) license (<https://creativecommons.org/licenses/by/4.0/>).

1. Introduction

The notion of the microgrid emerged almost twenty years ago with the aim of obtaining a more efficient use of electric energy when combining generation, conversion, and consumption together with the idea of decentralized production. Consequently, a great number of applications were reported, ranging from microgrids for large photovoltaic installations to microgrids adapted to factories in urban environments or designed for renewable energy-based power generation in rural areas without electricity [1].

Almost simultaneously, electric vehicles (EVs) began to penetrate the market in a rapid evolution in which the first models were immediately replaced by new alternatives, which in turn became obsolete in comparison with the later products offered by practically all car manufacturers that had decided to create their own EV. This spiral implied a continuous

variation in the electrical architecture of the EV and in the levels of current and voltage handled inside, and therefore it precluded the adoption of many production standards.

In a clear-cut contrast, the charging of EVs has remained in the same categorization envisaged in the first years, i.e., domestic charging, fast charging, and ultrafast charging. Domestic charging uses an on-board battery charger that is connected to the ac mains and requires several hours to complete the charging process. Fast charging is based on a dc voltage supply handling power between 50 kW and 150 kW, and it results in charging times between 10 and 30 min. Ultrafast charging is performed from a dc bus providing a minimum value of power of 350 kW, reducing the charging time to less than 10 min [2].

State of the Art and Objectives

In this context, specific microgrids for EV battery charging have been the subject of different studies in the last few years; they have in common the use of a medium voltage network (MV) as a primary energy source to satisfy the huge power demand in both fast and ultrafast charging [3,4]. Moreover, it is generally accepted to include an energy storage system in the electrical architecture of the charging station to support the EVs charging in the moments of peak power demand [5–7] and use a hybrid ac/dc microgrid to implement the architecture [8].

A detailed study of the charging infrastructure market is reported in [9], where dedicated on-board chargers are reviewed, charging standards are updated, and the technology of stations for high-power off-board charging is commented on. Nonetheless, other than a succinct description regarding off-board converter topologies, there is no information on the use of specific microgrids for battery charging.

There are several steps in the design of a microgrid for battery charging. The first one is to determine the power to be handled by the station and the number of charging points that will ensure a good quality of service [10]. A second issue is in regards to the design of the electrical architecture that can satisfy the power requirements. A subsequent aspect is modeling the microgrid as a state machine and establishing all its operating modes. From the latter point onwards, there are many degrees of freedom in the design, which depend on the approach used in the hierarchical control required in the implementation of the state machine. If power sharing is required, solutions reported in other types of microgrids can be employed, such as sliding mode control [11], distributed periodic event-triggered algorithms [12], and distributed hybrid control [13].

Based on a statistical analysis of real traffic data on a highway in the northeast of Spain, a hybrid microgrid was proposed for the electrical architecture of an ultrafast charging station (UFCS) whose steady-state operation was simulated in [14]. A block diagram of the microgrid is illustrated in Figure 1, where the MV grid supplies the station through a solid-state transformer (SST) [15] and the internal power distribution is carried out by means of an ac bus of 220 V and two dc buses of 600 V and 1500 V, respectively. The purpose of the 600 V dc bus is to insert renewable energy sources into the station, as depicted in Figure 1 by a wind turbine and a photovoltaic array. The 1500 V dc bus is the main dc bus and performs the charging in four points with a unidirectional converter in each one. The latter converter interfaces EV batteries with a nominal voltage in the range between 400 and 800 V.

Charging four EVs simultaneously requires a maximum power of 1.5 MW, assuming both 95% efficiency in the power converters and the support of the energy storage system (ESS). The ESS provides the extra current required in that situation and consists of a battery package and a supercapacitor module, which gives a hybrid characteristic to the system with the aim of relaxing the power demand in the batteries and increasing its lifetime [16–18]. Nonetheless, the insertion of the hybrid energy storage system (HESS) into the microgrid is not a simple task because it requires a detailed analysis of the operating modes and transitions among them [19], together with the design of the appropriate control regulating the dynamic behavior of the transitions and the voltage of the main bus. Finding a balance between an automatic transition in two operating modes and a precise control regulating the transition requires the use of a hierarchical control.

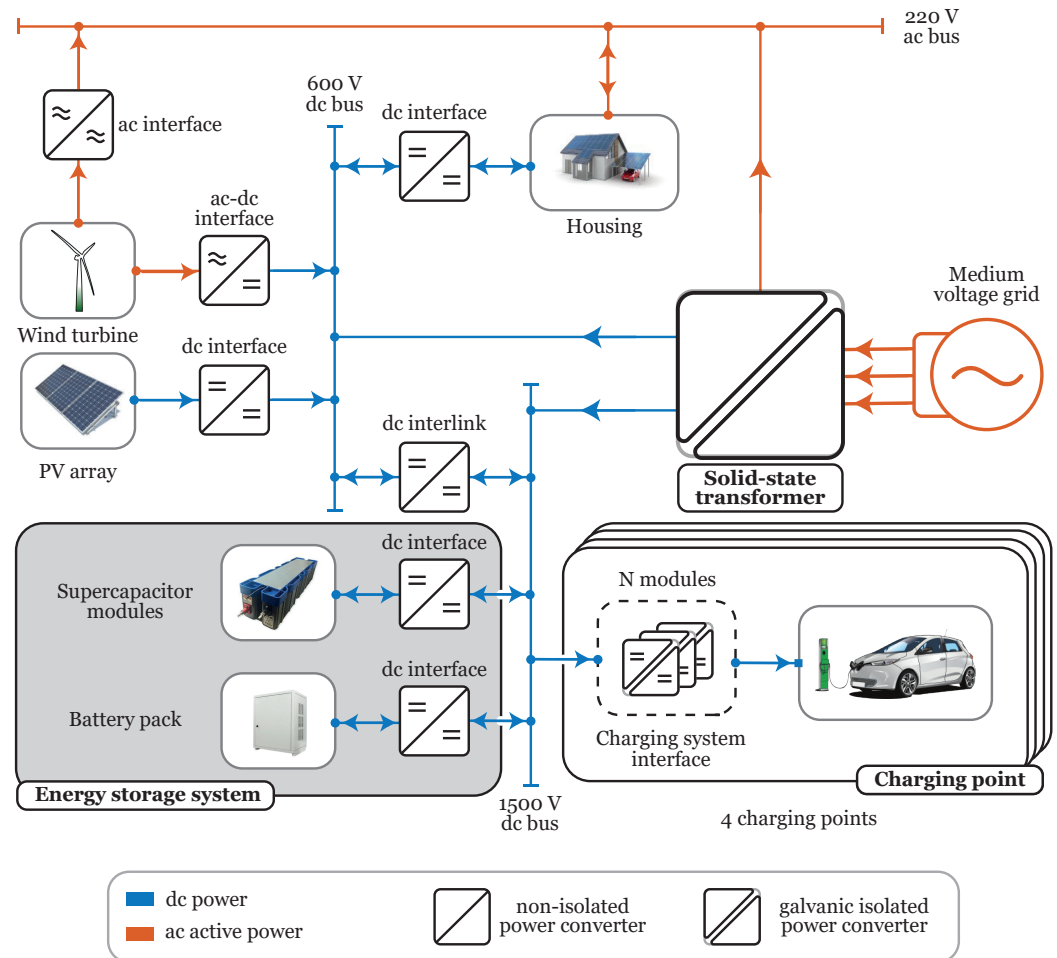


Figure 1. Electrical architecture of the ultrafast charging station studied in [14].

The main goal of this paper is to present the analysis, design, and simulation of a two-level hierarchical control to supervise and regulate the interaction of the HESS and the main dc bus in the microgrid for ultrafast charging, as depicted in Figure 1. The low level or primary control is devoted to the regulation of the converters involved in the interaction between the HESS and the main dc bus, while the high level or secondary control supervises the operating modes and establishes the references for the primary control.

The rest of this article is organized as follows. Section 2 presents an overview of the power distribution control, describing the interconnection of the HESS and main dc bus and explaining the corresponding operating modes and the role of the two layers of the hierarchical control. Section 3 shows the design of the primary control based on a cascade regulation strategy. Section 4 contains simulation results illustrating the regulated transition between the different modes that can emerge in the steady-state regime of one-day UFCS operation. Conclusions and research in progress are summarized in Section 5.

2. Overview of the Power Distribution Control

2.1. Hybrid Energy Storage System

Figure 2 shows a circuit diagram of the hybrid energy storage system (HESS) and its connection to a 1500 V dc bus. The HESS is composed of a battery pack and a supercapacitor module as energy storage devices (ESDs). Each ESD has its own bidirectional switching converter with the output port connected in parallel with the other converter. The current demanded by the charging points is supplied by the addition of the SST current and HESS current.

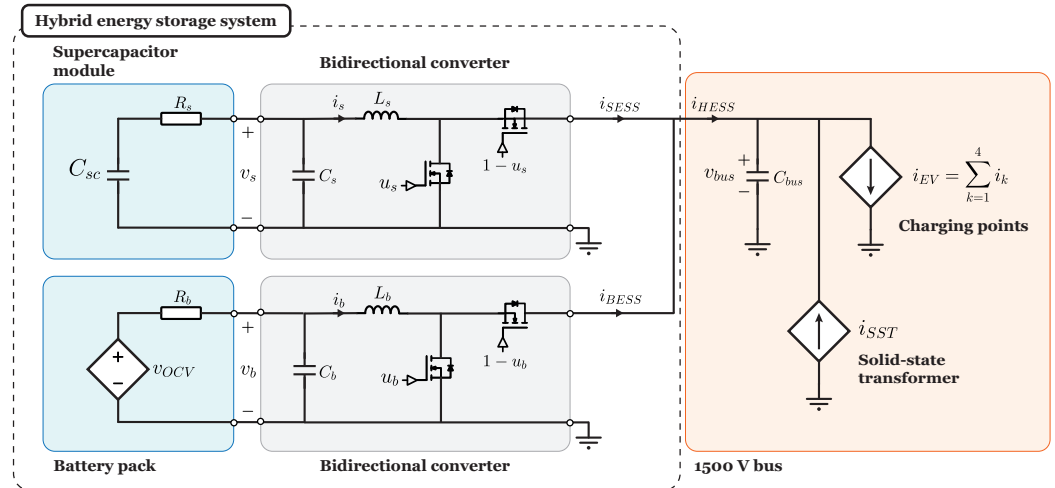


Figure 2. Circuit diagram of HESS and 1500 V dc bus.

A half-bridge converter is used to implement the power bidirectional converter for both ESDs. It operates as a voltage step-up converter when the power is transferred from the ESDs to the main bus and as a voltage step-down converter when the power flows in the opposite way. Thus, the direction of the currents i_s and i_b in Figure 2 defines the operation of the converter.

The current–voltage characteristics of the ESDs have been modeled using simple equivalent-circuit models. The supercapacitor is represented by a capacitance C_{sc} , accounting for the total capacitance, and the series resistance R_s represents the equivalent series resistance, which models the losses between the electrodes and the electrolyte. The battery pack model considers a dependent voltage source v_{OCV} , which is a function of the state of charge (SOC) of the pack, and the internal resistance R_b .

In our system, each ESD and its corresponding converter constitute an integrated module, namely, a battery energy storage system (BESS) and supercapacitor energy storage system (SESS). Thus, the total current of the HESS i_{HESS} results from the contributions of both modules.

$$i_{HESS} = i_{SESS} + i_{BESS} \quad (1)$$

As depicted in Figure 2, the current demanded by the charging points (ChPs) i_{EV} is supplied by the i_{HESS} and the SST current i_{SST} .

$$i_{HESS} + i_{SST} = i_{EV} \quad (2)$$

2.2. Operation Modes of HESS

The HESS control structure uses a two-level hierarchical approach. The lower level is composed of the primary controllers for the bidirectional power flow of each ESD.

The upper level is the secondary control and defines the operation modes when there is no power balance between the SST, the ChPs, and the HESS. The secondary control also establishes the references for the different primary controllers of the lower level in each operating mode.

Figure 3 summarizes the operation modes of the HESS and their respective transition conditions. This state machine is a reflection of the operating modes defined in the centralized control in [14], which were classified as grid-tied and islanded operating modes. For the centralized control, the transition among UFCS operating modes is carried out through power balancing in the 1500 V dc bus, establishing the same Equation (2) in terms of power. For grid-tied operation, there are four operating modes, namely, direct, complementary, limited loading, and standby. If there are no EVs to charge, the UFCS is in the standby mode and intends to keep the ESDs at optimal levels by charging them constantly. The direct loading mode appears when the power supplied by the SST is sufficient to

feed the demand of all ChPs. The remaining power from the SST is used to charge the HESS when necessary. If the power of the ChPs exceeds the maximum power of the SST, additional power will be injected from the HESS to supply the power balance. This will set the complementary loading mode in the UFCS if the combined power from the SST and HESS maintains the power balance; otherwise, it will establish the limited loading mode, in which the demanded power in ChPs is limited to the maximum power of the SST and HESS.

In absence of power from the SST, the UFCS will work in islanded operation, in which the HESS will be the main supplier to the ChPs. This operation of the UFCS has three modes depending on the SOC of the battery pack: the autonomous, burnout, and disconnection modes. The first one is the default mode in islanded operation and supplies the ChPs up to the maximum power of the HESS. If the SOC of the battery pack falls under 40% during the autonomous mode, the UFCS will enter into the burnout mode. In this condition, the UFCS will supply only the EVs that are already charging and will stop providing service to the future EVs. After fulfilling the charging of the EVs, no service is provided until the SST is active again.

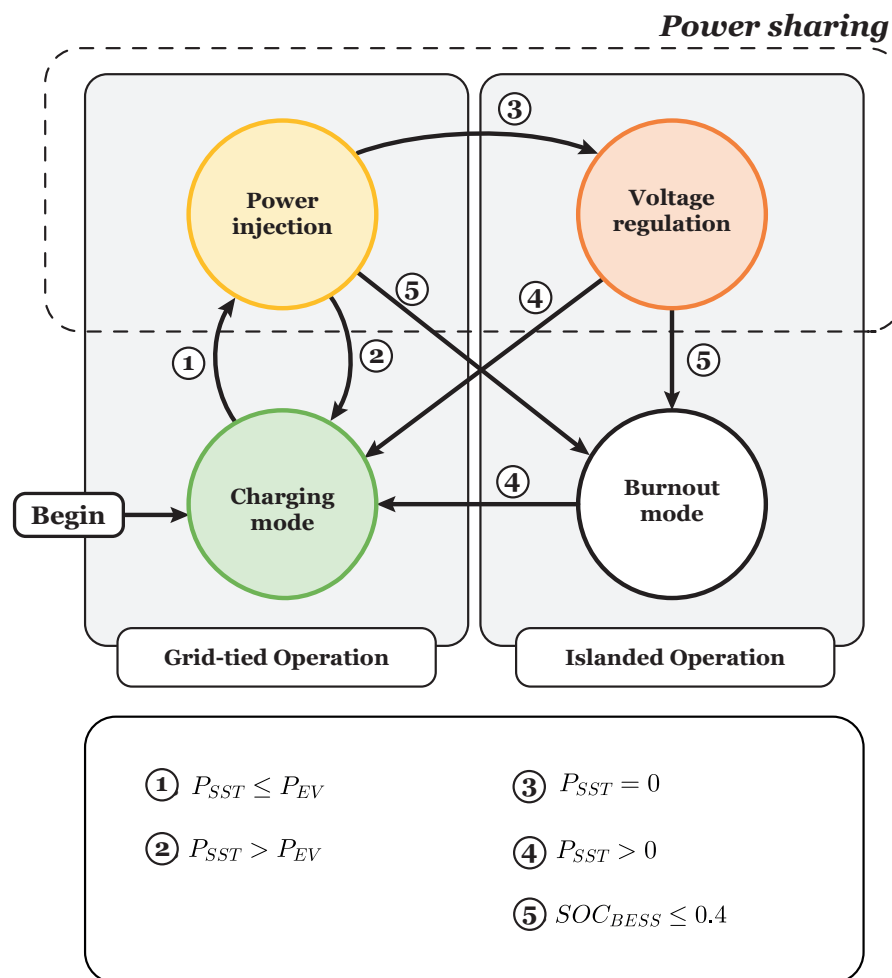


Figure 3. State machine with operating modes of HESS.

Thus, the charging mode in Figure 3 corresponds to the direct loading and standby modes. The power injection mode corresponds to complementary and limited loading, and the voltage regulation mode in turn corresponds to the autonomous one. Finally, the burnout mode of the HESS represents the burnout and disconnection modes.

3. Primary Controller Design

The primary controller has a cascade control, where the inner loop is a sliding mode control (SMC) with a switching surface based on the converter inductor current. Each ESS module has its own switching surface $S_j(i_j)$, which is valid for both the voltage step-up and step-down modes and is given by Equation (3).

$$S_j(i_j) = i_{ej} - i_j \quad (3)$$

The sub-index j corresponds to sub-indexes b and s for the battery pack inductor current and supercapacitor module inductor current, respectively. The variable i_{ej} is the current reference given by the outer control loop, as illustrated in Figure 4.

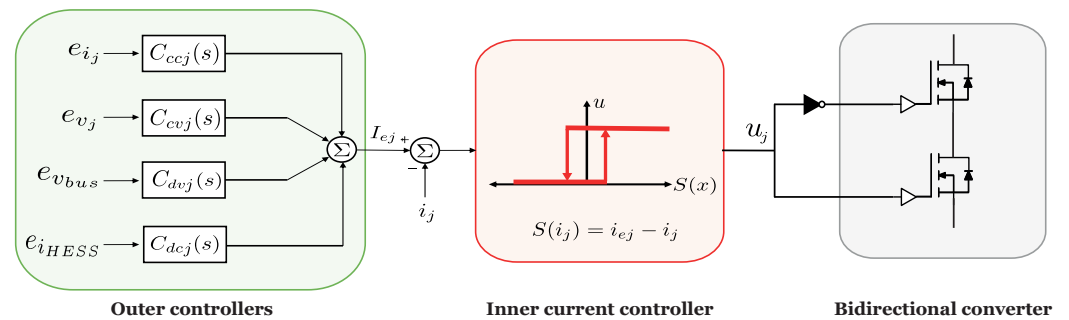


Figure 4. Cascade control loop structure.

The choice of the current inner loop allows for the use of a modular design structure that is implementable in each ESS module with the possibility of connecting similar modules to expand the capacity of the HESS. In addition, the converter current is related to all the other state variables present in the module, ensuring a complete control over the voltages and currents at the converter ports.

3.1. Inner Current Controller

The set of equations that describe the behavior of the system illustrated in Figure 2 is summarized in Equations (4)–(6) for the SESS module, BESS module, and main dc bus. The control variables u_b and u_s are binary signals taking the values 1 or 0 for power transistor activation and deactivation, respectively.

$$L_s \frac{di_{L_s}}{dt} = v_s - v_{bus}(1 - u_s) \quad (4a)$$

$$C_s \frac{dv_s}{dt} = \frac{v_{sc} - v_s}{R_s} - i_{L_s} \quad (4b)$$

$$C_{sc} \frac{dv_{sc}}{dt} = \frac{v_s - v_{sc}}{R_s} \quad (4c)$$

$$L_b \frac{di_{L_b}}{dt} = v_b - v_{bus}(1 - u_b) \quad (5a)$$

$$C_b \frac{dv_b}{dt} = \frac{v_{ocv} - v_b}{R_b} - i_{L_b} \quad (5b)$$

$$C_{bus} \frac{dv_{bus}}{dt} = i_{L_s}(1 - u_s) + i_{L_b}(1 - u_b) + i_{SST} - i_{EV} \quad (6)$$

The surface in (3) induces sliding motions in the system using the control law in (7) [20–22]. The value Δ corresponds to a hysteresis band that will provide the required finite switching frequency in a laboratory implementation and lead to a peak-to-peak current ripple of 2Δ in the inductors.

$$f(x) = \begin{cases} 0, & \text{if } S_j(x) < -\Delta \\ 1, & \text{if } S_j(x) > +\Delta \end{cases} \quad (7)$$

with $j = [b, s]$.

The existence of a sliding motion implies the accomplishment of the invariance condition [23] for each ESS module, resulting in the equivalent control u_{jeq} expressed in (8) and the corresponding ideal sliding dynamics of the HESS given by (9).

$$u_{jeq} = 1 - \frac{v_j}{v_{bus}} + \frac{L_j}{v_{bus}} \frac{di_{ej}}{dt} \quad (8)$$

$$i_s = i_{es} \quad (9a)$$

$$i_b = i_{eb} \quad (9b)$$

$$\frac{dv_{sc}}{dt} = \frac{1}{C_{sc}} \frac{v_s - v_{sc}}{R_s} \quad (9c)$$

$$\frac{dv_s}{dt} = \frac{1}{C_s} \left(\frac{v_{sc} - v_s}{R_s} - i_{L_s} \right) \quad (9d)$$

$$\frac{dv_b}{dt} = \frac{1}{C_b} \left(\frac{v_{OCV} - v_b}{R_b} - i_{L_b} \right) \quad (9e)$$

$$C_{bus} \frac{dv_{bus}}{dt} = \left(i_{es} \left[1 - \frac{v_s}{v_{bus}} + \frac{L_s}{v_{bus}} \frac{di_{es}}{dt} \right] + i_{eb} \left[1 - \frac{v_b}{v_{bus}} + \frac{L_b}{v_{bus}} \frac{di_{eb}}{dt} \right] + i_{SST} - i_{EV} \right) \quad (9f)$$

Linearizing the ideal sliding dynamics around the equilibrium points $\bar{I}_s, \bar{V}_s, \bar{I}_b, \bar{V}_b$, and \bar{V}_{bus} yields the linearized Equation (10) for the entire system.

$$\tilde{i}_s = \tilde{i}_{es} \quad (10a)$$

$$\tilde{i}_b = \tilde{i}_{eb} \quad (10b)$$

$$\frac{d\tilde{v}_{sc}}{dt} = \frac{1}{C_{sc}} \frac{\tilde{v}_s - \tilde{v}_{sc}}{R_s} \quad (10c)$$

$$\frac{d\tilde{v}_s}{dt} = \frac{1}{C_s} \left(\frac{\tilde{v}_{sc} - \tilde{v}_s}{R_s} - \tilde{i}_{L_s} \right) \quad (10d)$$

$$\frac{d\tilde{v}_b}{dt} = -\frac{1}{C_b} \left(\frac{\tilde{v}_b}{R_b} + \tilde{i}_{L_b} \right) \quad (10e)$$

$$C_{bus} \frac{d\tilde{v}_{bus}}{dt} = B_s \tilde{i}_{es} + A \tilde{v}_s - [A_s B_s] \tilde{v}_{bus} - A_s L_s \tilde{i}_{es} + B_s \tilde{i}_{eb} + A_b \tilde{v}_{bat} - [A_b B_b] \tilde{v}_{bus} - A_b L_b \tilde{i}_{eb} + \tilde{i}_{SST} - \tilde{i}_{EV} \quad (10f)$$

where

$$\tilde{i}_{es} \triangleq \frac{di_{es}}{dt}, \quad \tilde{i}_{eb} \triangleq \frac{di_{eb}}{dt}, \quad A_s = \frac{\bar{I}_s}{\bar{V}_{bus}}, \quad B_s = \frac{\bar{V}_s}{\bar{V}_{bus}}, \quad A_b = \frac{\bar{I}_b}{\bar{V}_{bus}}, \quad B_b = \frac{\bar{V}_b}{\bar{V}_{bus}}$$

To facilitate the control design, Table 1 provides a summary of seven transfer functions $G_{pqj}(s)$ derived from (9) in which the inductor currents are related to another state variable. The nomenclature of the transfer functions uses three sub-indexes: the first one “ p ” differentiates the direction of the power flow, i.e., “ c ” is employed when the inductor current flows from the bus to the ESD, while “ d ” is used for the opposite direction. The second one, “ q ”, indicates the type of state variable being controlled, i.e., “ c ” for the current and “ v ” for the voltage. The ESS modules in turn are referenced with “ s ” for the SESS module and “ b ” for the BESS module.

Table 1. Transfer functions of the linearized sliding dynamics.

| Transfer Function | Nomenclature | Description |
|---------------------------------|--------------|---|
| $\frac{I_s(s)}{I_{es}(s)}$ | $G_{ccs}(s)$ | 1 |
| $\frac{V_s(s)}{I_{es}(s)}$ | $G_{cvs}(s)$ | $-\frac{\frac{1}{C_s}}{s + \frac{1}{C_s R_s}}$ |
| $\frac{I_{HESS}(s)}{I_{es}(s)}$ | $G_{dcs}(s)$ | B_s |
| $\frac{V_{bus}(s)}{I_{es}(s)}$ | $G_{dvs}(s)$ | $\frac{-A_s L_s s^3 + (B_s - A_s E L_s) s^2 + (B_s E - A_s F L_s - \frac{A_s}{C_s}) s + (B_s F - \frac{A_s D}{C_s})}{(C_{bus} s + A_s B_s)(s^2 + E s + F)}$ |
| $\frac{I_b(s)}{I_{eb}(s)}$ | $G_{ccb}(s)$ | 1 |
| $\frac{V_b(s)}{I_{eb}(s)}$ | $G_{cvb}(s)$ | $-\frac{\frac{1}{C_b}}{s + \frac{1}{C_b R_b}}$ |
| $\frac{I_s(s)}{I_{eb}(s)}$ | $G_{dcb}(s)$ | $-\frac{B_b}{B_s}$ |

3.2. Charging Mode

The charging mode of the HESS is managed by a unified scheme control for both modules with the CC-CV standard method. Each ESD is charged using the control diagram shown in Figure 5. In the CC state, the controller $C_{ccj}(s)$ produces a smooth start-up in order to reduce the disturbance of the charging process in the dc bus by means of an integrator, which results in a first-order dynamic behavior in the inductor current.

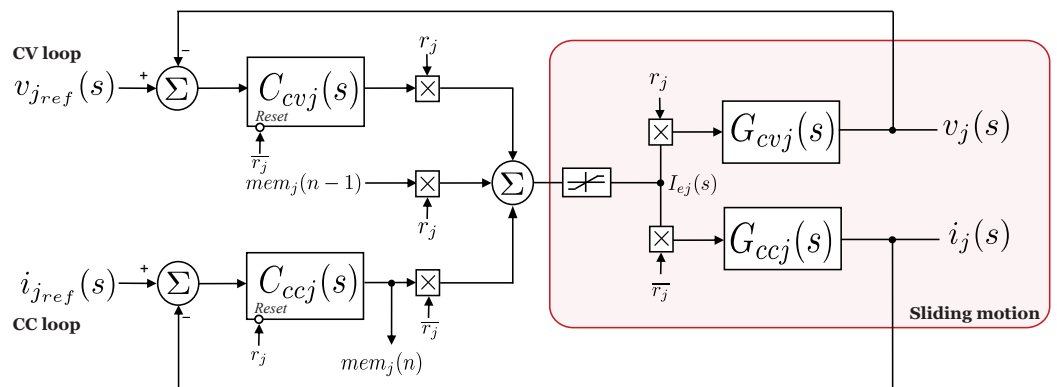


Figure 5. Charging control loop implementing the CC-CV protocol.

In the CV stage, the controller $C_{cvj}(s)$ is also an integrator due to both the slight constraints imposed by $G_{cvj}(s)$ and the smooth transition between CC and CV stages. The binary variable r_j and its opposite \bar{r}_j are used in the charging process. Thus, $r_j = 0$ enables the charging process for the CC stage, while $r_j = 1$ allows it for the CV stage. In addition, both variables are used to reset the controllers $C_{cvj}(s)$ and $C_{ccj}(s)$ during the CC to CV transition. The reset occurs when a zero appears in the reset input. The auxiliary memory variable mem_j stores the output value ($mem_j(n - 1)$) of the active control at the instant before a transition and keeps the value in the next mode ($mem_j(n)$) in order to achieve a smooth transition between controllers.

3.3. Power Sharing Strategy

Figure 6 illustrates the control diagram for the power sharing strategy involving power injection in a grid-tied operation and voltage regulation in case of an islanded operation. In both modes, the power sharing control operates in the same way. Namely, the SESS is in charge of regulating the voltage in the dc bus (yellow region with controller $C_{dvs}(s)$) or delivering a power reference to the bus in case of a power injection (orange region with controller $C_{dcs}(s)$ and reference generated by the secondary control). In the meantime, the BESS is responsible for cancelling the SESS current in a steady state through controller

$C_{dcb}(s)$. Thus, in terms of energy, it is the BESS that supplies the desired power to the bus, while the peaks and disturbances are absorbed by the SESS. Therefore, for the design of the controllers of current injection and voltage regulation modes, it must be taken into account that the SESS dynamics has to be faster than that of the BESS. The resulting dynamics from the interaction between the SESS and the BESS modules decouples the power demand of the ChPs into low-frequency (BESS current) and high-frequency (SESS current) components without resorting to filtering or estimating [11].

The binary variable m_{sc} and its opposite \bar{m}_{sc} are used to change between the two operating modes of the SESS. With that in mind, $m_{sc} = 0$ corresponds to power injection and $m_{sc} = 1$ to voltage regulation. Moreover, both variables also reset the controller to preclude saturation in their outputs. The auxiliary memory variables mem_s and mem_v store the output value of the voltage regulation and power injection controllers, respectively, and operate in the same way as mem_j does in the charging control case. The controller $C_{dcb}(s)$ does not require a secondary memory because it works continuously. A low-pass filter with a 10 kHz cutoff frequency has been applied to the i_{HESS} and i_s currents to obtain their respective dc components and a continuous-time error signal for the controllers.

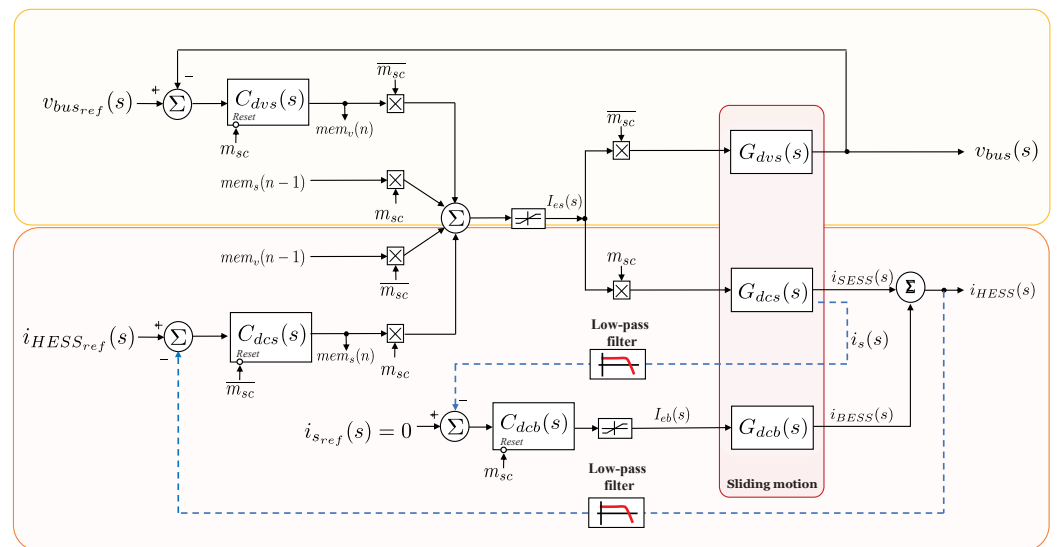


Figure 6. Power sharing control loop implemented for power injection and voltage regulation modes.

3.4. Outer Controller Design and Constrains

Most of the controllers shown in Figures 5 and 6 have been based on a pure integrator controller [11]. This type of controller is of special interest since some of the transfer functions presented in Table 1 are mainly of a constant type or first order leading to the first-order dynamic behavior of the regulated system. The gain of the integrator controller can be obtained looking at the closed-loop pole of a desired first-order transfer function as follows:

$$K_i = \frac{1}{G(0)\tau_d} \tag{11}$$

where $G(0)$ is the static gain of the transfer function and τ_d is the desired constant time.

For both $C_{ccj}(s)$ and $C_{cvj}(s)$ controllers of the charging mode and for the $C_{dcb}(s)$ controller cancelling the SESS current, a settling time of 5 s has been considered. In contrast, a settling time of 100 ms has been designed for the power injection controller $C_{dcs}(s)$. With respect to the dc bus voltage regulation, a value of $C_{bus}(s)$ of 2.2 F is assumed in order to reduce the impact of the power demand of the ChPs when an EV arrives to the station. Thus, the controller for regulating the voltage bus $C_{dvs}(s)$ has been designed in the frequency domain with a phase margin of 74.2° obtaining a settling time of 10 ms and an overshoot of 10%. Table 2 summarizes the outer converter transfer functions with the same nomenclature used in Table 1.

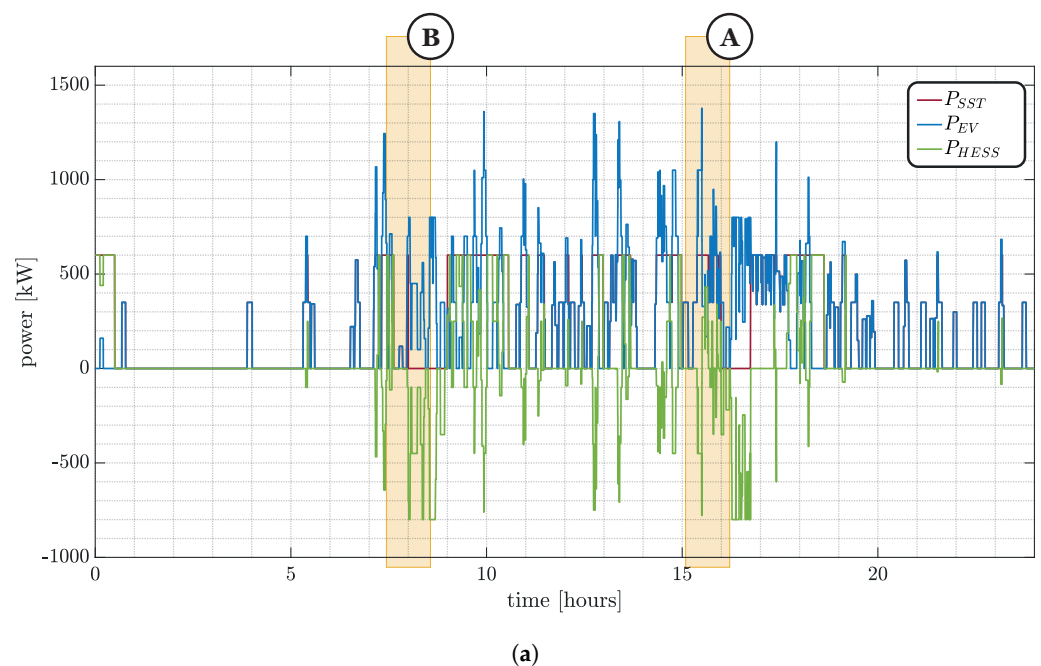
Table 2. Outer controllers' values in Figures 5 and 6.

| Nomenclature | Description |
|--------------|---------------------------|
| $C_{ccs}(s)$ | $\frac{1}{s}$ |
| $C_{cvs}(s)$ | $\frac{12.5}{s}$ |
| $C_{ccb}(s)$ | $\frac{1}{s}$ |
| $C_{cwb}(s)$ | $\frac{4.8}{s}$ |
| $C_{dcs}(s)$ | $\frac{115.74}{s}$ |
| $C_{dvs}(s)$ | $\frac{937.5(s+12.5)}{s}$ |
| $C_{dcb}(s)$ | $\frac{1}{s}$ |

4. Simulation Results

In order to validate the theoretical analysis in Section 3 by means of simulation, it is necessary to study the transitions among operation modes superposed to the steady-state behavior of the UFCS. For that reason, we will use the data of one-day steady-state simulation given by the software developed in [14] as a starting point. This implies the selection of time intervals to visualize different operating points and transitions of the HESS and to obtain information about the transferred power between elements in the main bus, the SOC of the battery bank, and the occupancy of the ChPs. This information will be used in a PSIM simulation of the dynamic transitions among the operating modes, also taking into account the different time scales between static and dynamic simulations, which require time steps of 1 s and 0.1 μ s, respectively.

Figure 7 shows a steady-state simulation of the UFCS for one day of operation, providing service to 180 EVs. Figure 7a shows the power balance in the main bus. The blue profile shows the consumption of the ChPs, while the red one depicts the power delivered by the grid, and the green one illustrates the power processed by the HESS. Consequently, Figure 7b shows the sequence of operating modes of the UFCS and allows for the selection of the transition points. Finally, Figure 7c shows the SOC evolution of the battery pack.

**Figure 7.** Cont.

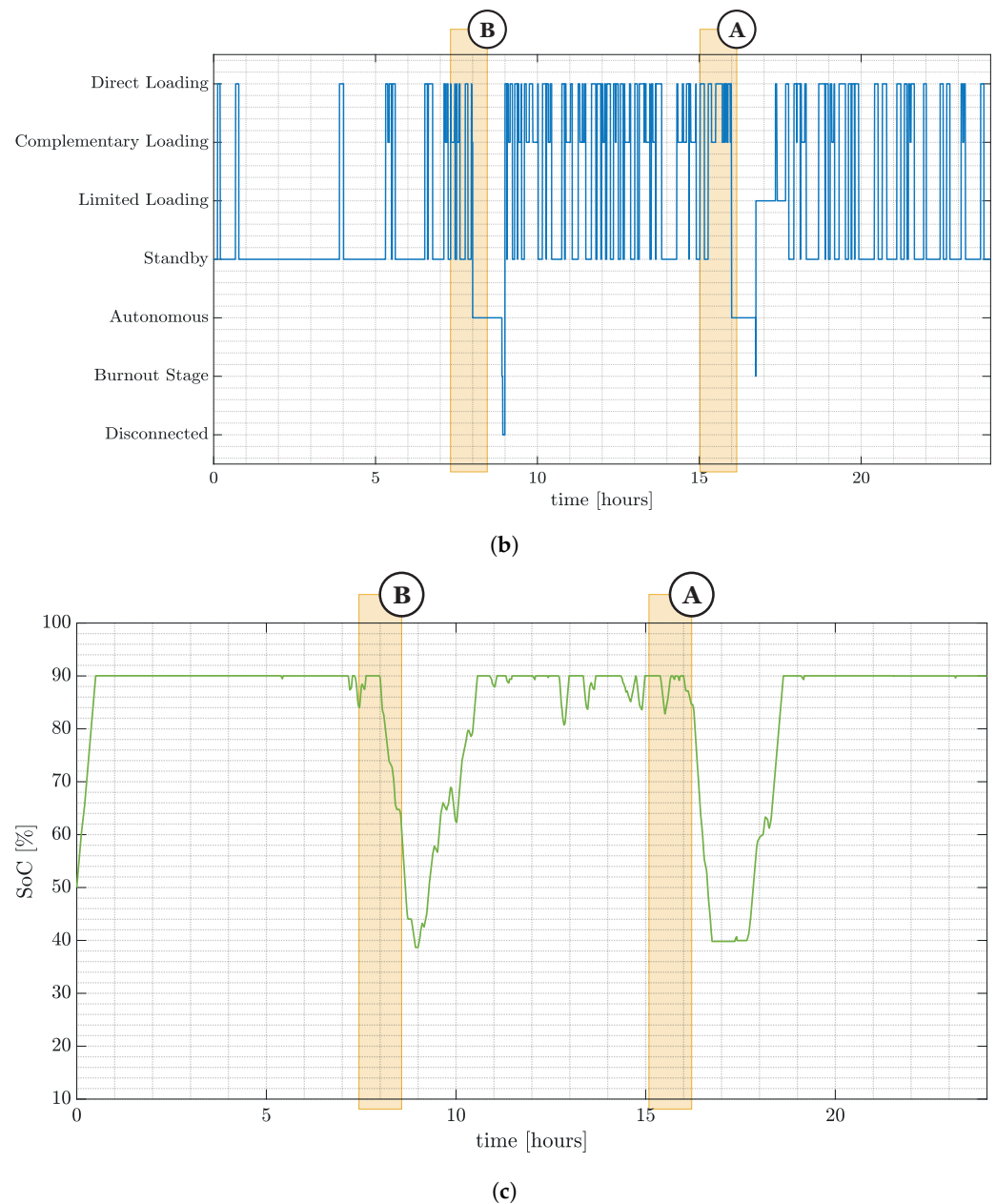


Figure 7. Steady-state simulation of the UFCS for one-day operation providing service to 180 EVs with two highlighted time-interval A and B: (a) power flow in the main bus among HESS, SST, and the ChPs; (b) sequence of operation modes of the UFCS; (c) state of charge of the battery bank.

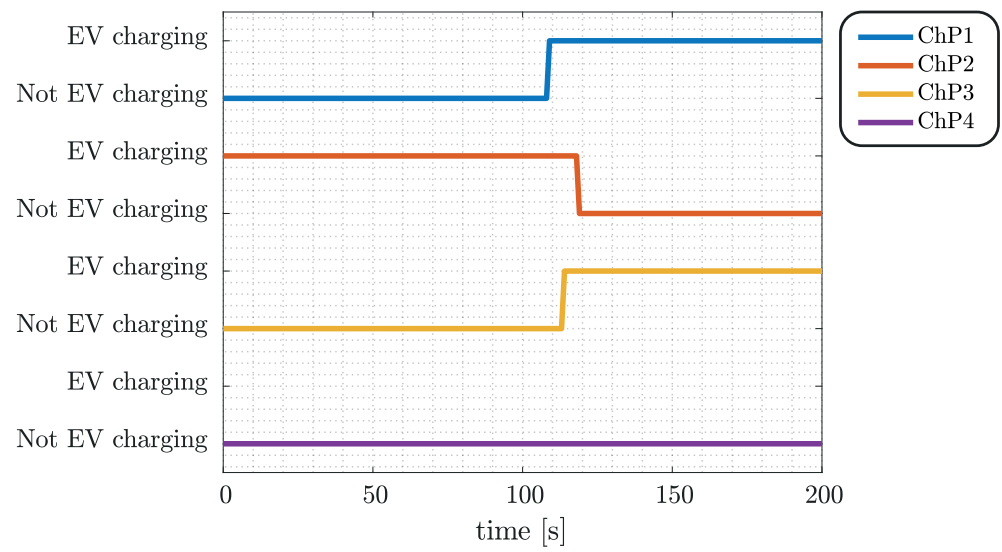
To illustrate the islanded operation of the station, two disconnections of the SST have been produced at different intervals: the first one lasting 1 h at 8:00 a.m. and the second one lasting 45 min at 4:00 p.m. Points A and B in Figure 7 have been selected for validation, and they correspond to the operation and transition of the HESS during grid-connected and islanded operations, respectively.

For both simulations, maximum power levels have been established, namely, 600 kW for the SST, 1.5 MW for the discharging process in the BESS, and 350 kW for each ChP. Furthermore, in steady-state simulation, the HESS is modeled as a battery, while the supercapacitor contribution is neglected.

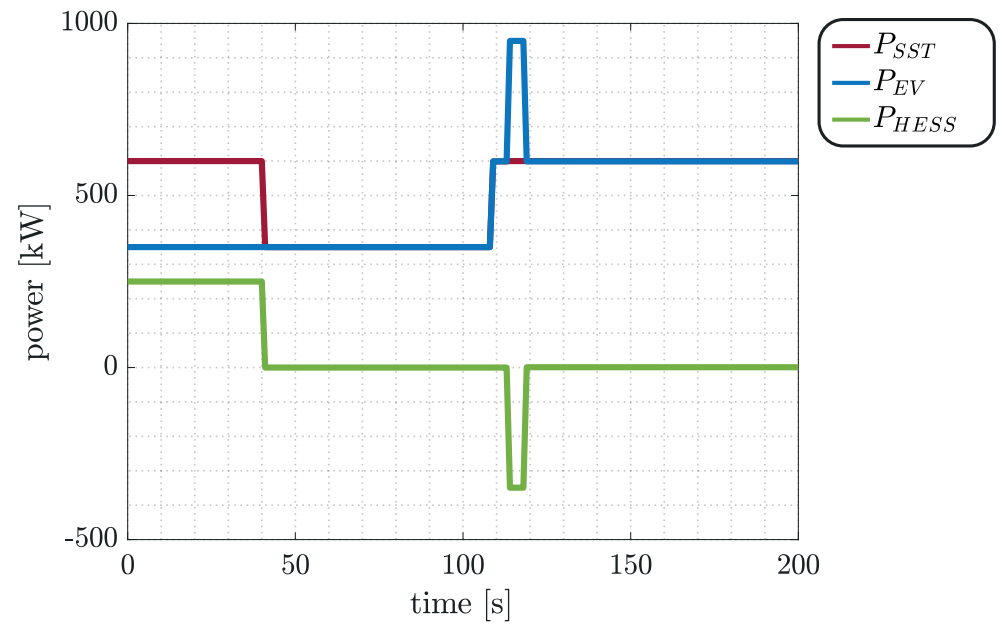
4.1. Transitions in Grid-Connected Operation Mode

Figure 8 illustrates the time interval A corresponding to the grid-connected operation of the UFCS when supplying three EVs. Figure 8a displays the occupied charging points

that are delivering energy. The sequence is as follows: while ChP2 is occupied, a new vehicle arrives at ChP1, and, shortly after, another one occupies ChP3. The power demand of these points is shown in Figure 8b. Initially, when only ChP2 is absorbing power, the remaining available power from the SST is used to recharge the HESS. It can be observed that the power demanded by the ChPs does not exceed the grid limit of 600 kW until the arrival of the second EV, which results in a direct charging operation. Hence, the HESS does not inject power until the arrival of a third EV increases the demand. At that moment, the HESS contributes to the charging process and the system transitions to the complementary charging mode [14]. Once the EV at ChP2 is charged, the demand falls below the SST's maximum power and the system returns to direct charging mode, as depicted in Figure 8c.

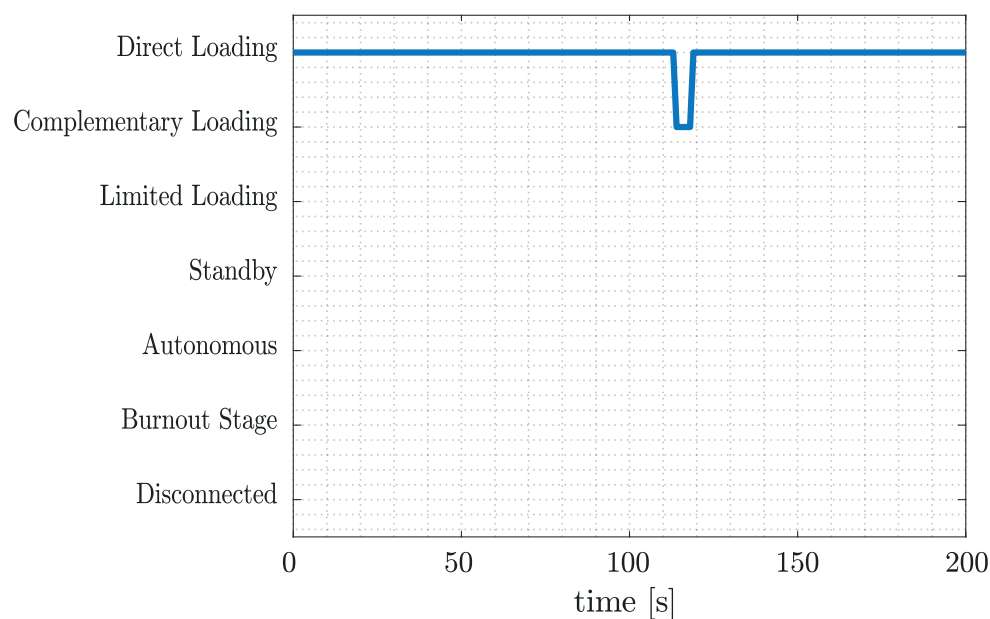


(a)



(b)

Figure 8. Cont.



(c)

Figure 8. Detail of interval A in Figure 7: (a) ChPs occupancy, (b) power flow, (c) sequence of UFCS operating modes.

Figures 9–11 depict the results of the dynamic simulation using the parameter values in Table 3 for the circuit components of the HESS.

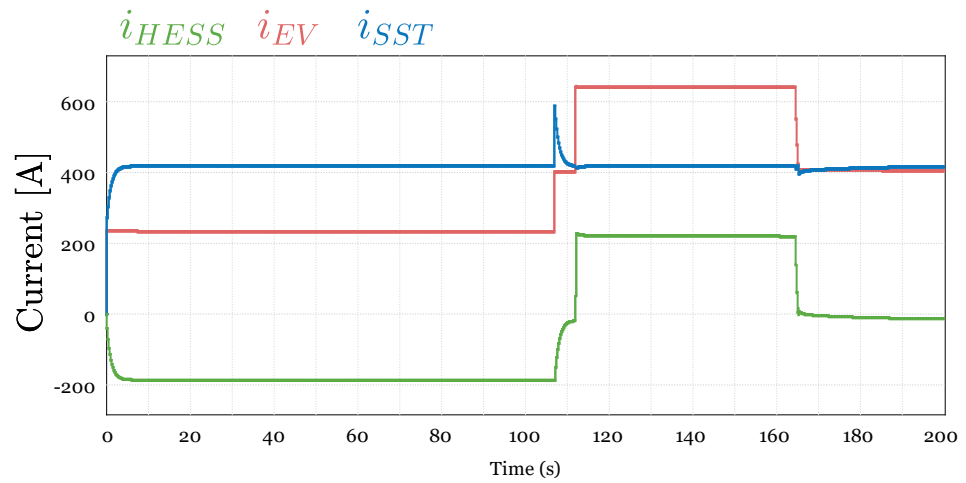
Table 3. Parameters for the circuit model in Figure 2.

| Parameter | Value |
|---------------|---------------|
| C_{sc} | 29 F |
| C_s | 20 μ F |
| R_s | 46 m Ω |
| V_s nominal | 600 V |
| L_s | 800 μ H |
| C_b | 20 μ F |
| R_b | 15 m Ω |
| V_b nominal | 750 V |
| L_s | 1200 μ H |
| C_{bus} | 2.2 F |

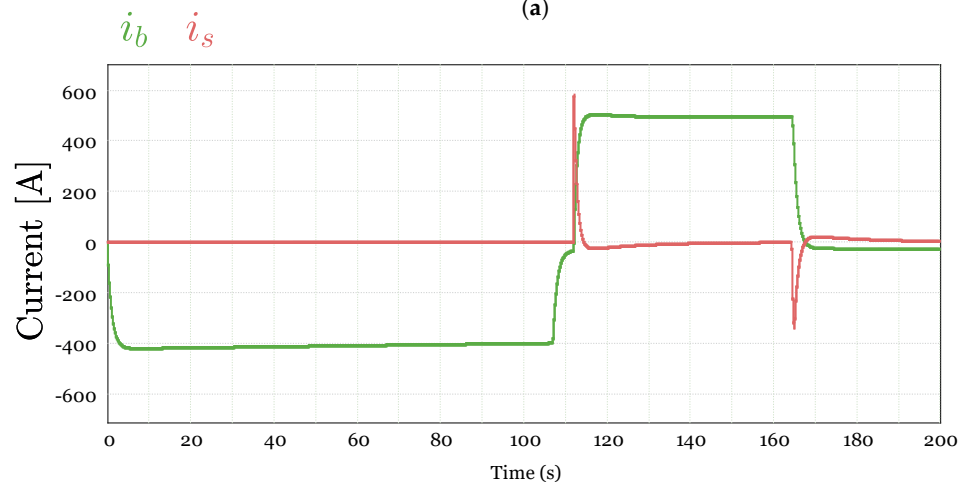
Figure 9a shows the inductor currents i_b and i_s in the BESS and SESS modules, respectively, while Figure 9b depicts the current flow in the main bus. The HESS is not delivering power to the bus at the beginning, and current I_2 demanded by the EV of ChP2 (see Figure 11) is supplied by the SST, as the system is in the charging mode. The power flows to the BESS as in Figure 7b with the smooth start-up dynamics predicted in Section 3.

Figure 10 illustrates the bus voltage, which is regulated to 1500 V with the contributions of both the SST and battery voltage v_b , which is slowly increasing during the charging mode and slowly decreasing during the power injection. The power distribution strategy can be observed at the arrival of the last vehicle in second 112 when the demand exceeds the limit imposed on the SST. The interaction of the HESS modules decoupling the demand of the ChPs towards each ESD can be appreciated.

Finally, Figure 11 depicts the current injected into each ChP. This graph can be compared with Figure 7a, which shows which ChP is actually active supplying an EV.



(a)



(b)

Figure 9. PSIM simulation during interval A showing the current flow: (a) in the main bus; (b) in the HESS.

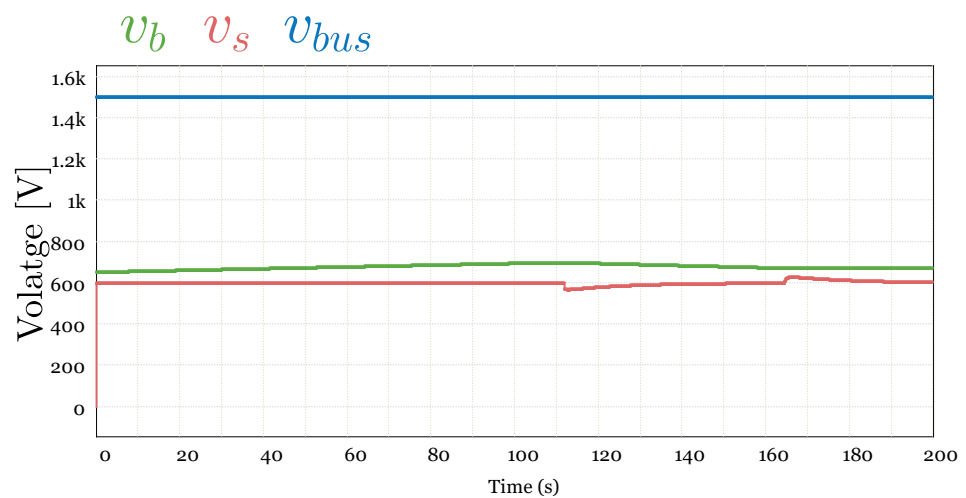


Figure 10. Bus voltage and ESD voltages during interval A.

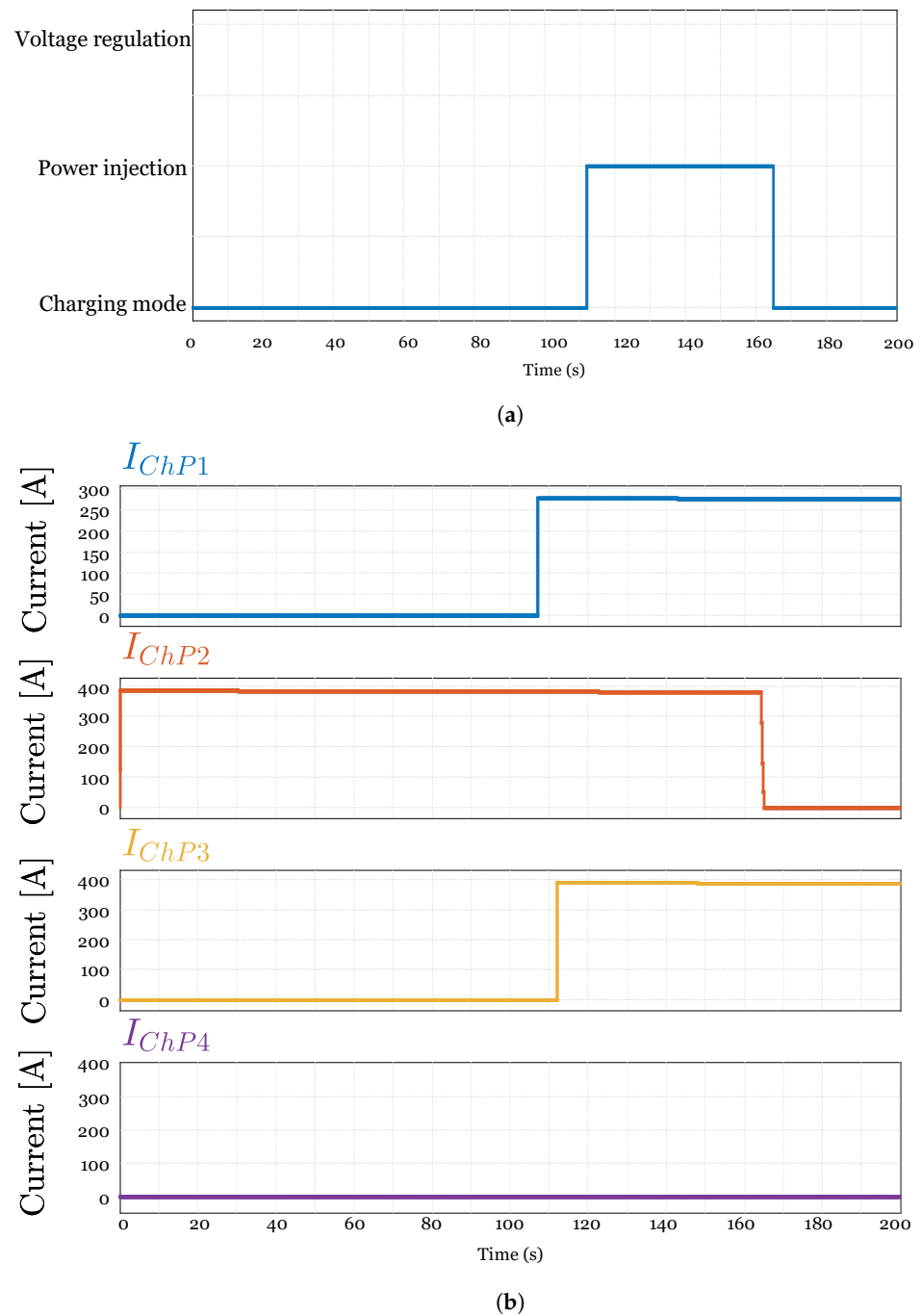
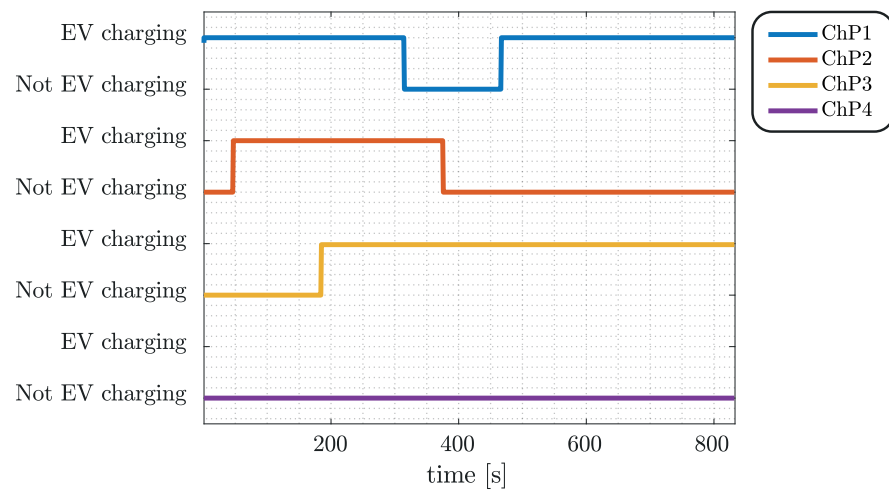


Figure 11. Operating modes of the HESS in interval A: (a) operation modes of the HESS; (b) current supply of ChPs.

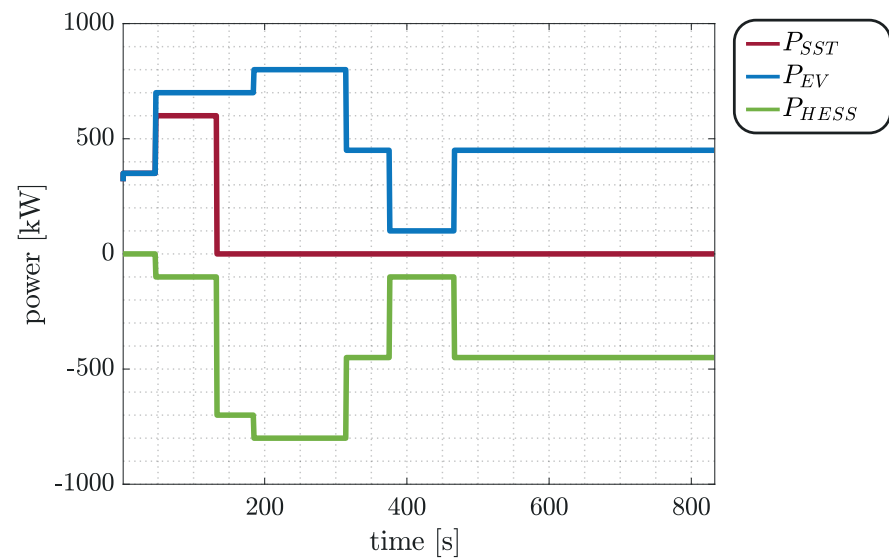
4.2. Transitions in Islanded Operation

Figure 12 shows the steady-state simulation of interval B, and Figure 13 shows the results of the dynamic simulation corresponding to the transition from the charging mode to the power injection mode in the presence of the SST and then the passage to the voltage regulation mode after a shutoff of the grid.

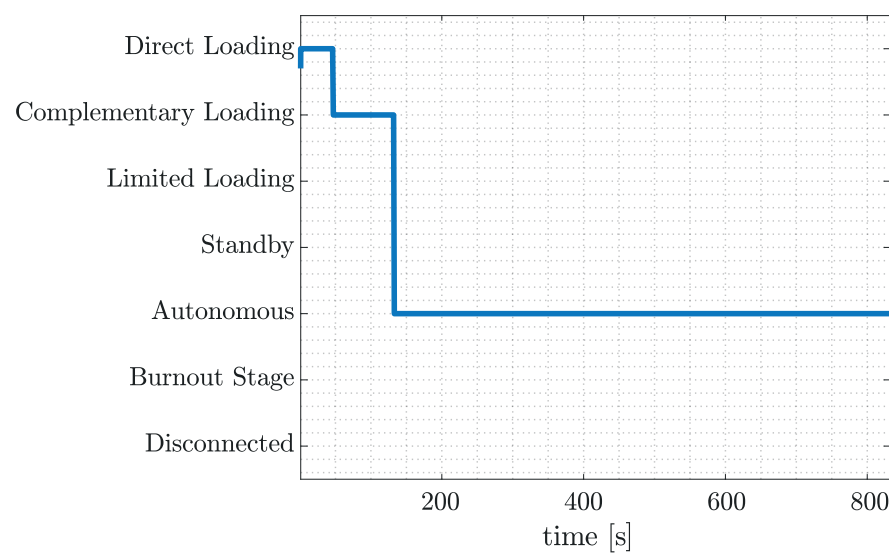
When initially only ChP1 is occupied, the SST supplies all the required current, and the energy surplus allows the battery to charge. The arrival of a second electric vehicle at ChP2 requires more power than that available in the SST, which provokes the transition to the power injection mode.



(a)



(b)



(c)

Figure 12. Details of interval A in Figure 7: (a) ChPs occupancy, (b) power flow, (c) sequence of UFCS operating modes.

A grid shutoff can be observed in second 130 of the simulation in Figure 13a, which implies that current i_{SST} is zero. The voltage regulation mode activates the SESS module, causing an initial power peak. Subsequently, the battery injects the required current, nullifying the contribution of the supercapacitor, as shown in Figure 13b. In order to maintain the nominal voltage of the supercapacitor, the battery injects an extra current after the transition to compensate for the capacitance loss of the former. In addition, Figure 14 illustrates the bus voltage, which is regulated to 1500 V with the contribution of both the battery and supercapacitor. Finally, the corresponding supply of the charging points and the operating modes of the HESS are depicted in Figure 15.

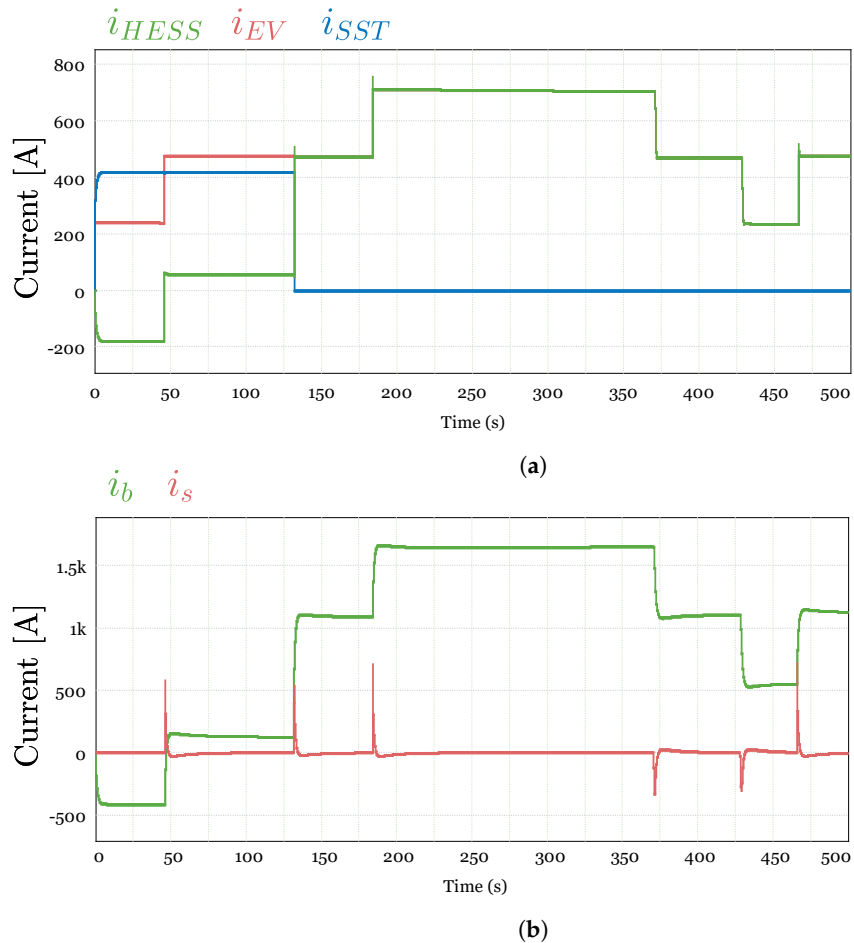


Figure 13. PSIM simulation during interval B showing the current flow: (a) in the main bus; (b) in the HESS.

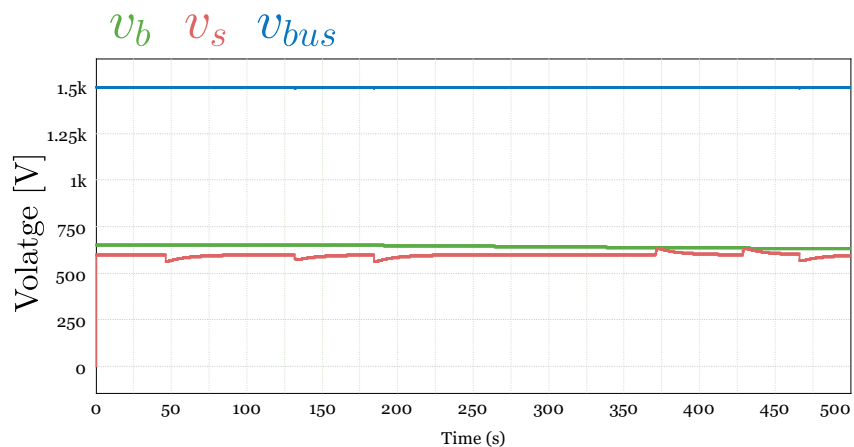
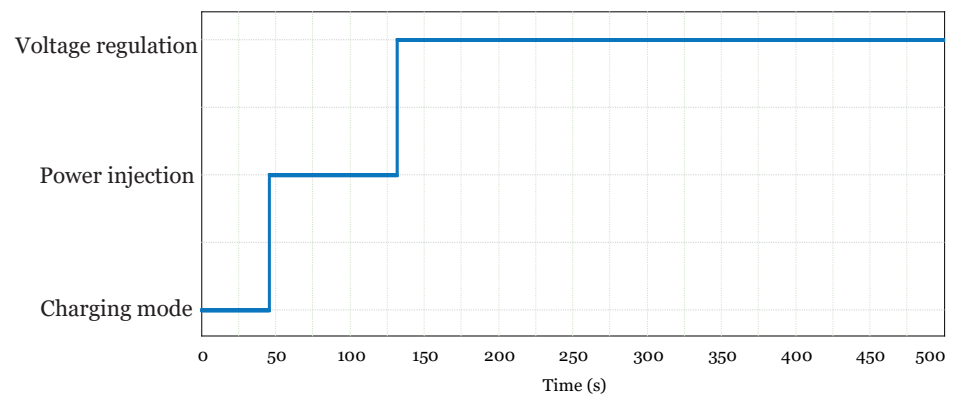
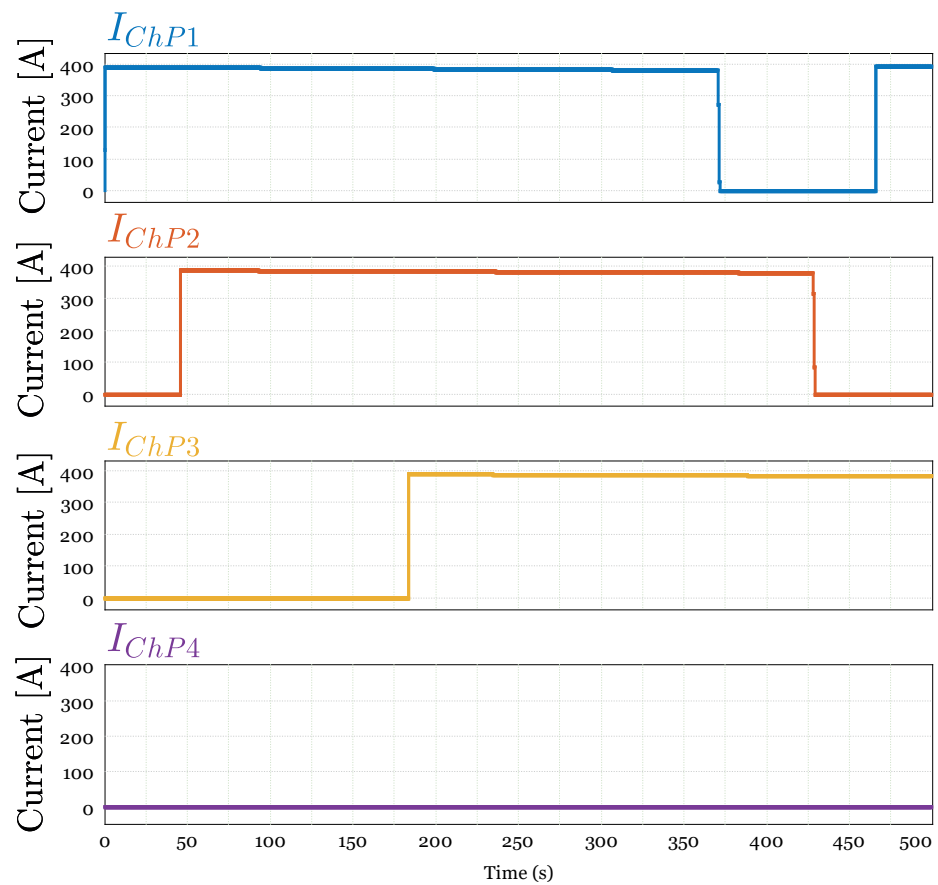


Figure 14. Bus voltage and ESD voltages during interval B.



(a)



(b)

Figure 15. Operating modes of the HESS in interval B: (a) current supply of ChPs. (b) operation modes of the HESS.

5. Conclusions

This paper has presented the regulated transitions among the different operating modes of a hybrid microgrid devoted to the ultrafast charging of electric vehicles. The operating modes represent the interaction between the primary energy input source (ac grid), the hybrid energy storage system (HESS), and the main dc bus of the microgrid.

The theoretical predictions of the transitions have been validated by means of PSIM simulations that use parametric information and appropriate time scales derived from the simulation of the steady-state operation of the charging station.

The transitions are regulated by a two-level hierarchical control method whose superior level supervises the operating mode that is underway and establishes the passage to

the next mode according to a state machine design. The control of the ongoing mode and the regulation of the transitions are performed by the low layer of the hierarchical control using a two-loop control approach.

The inner loop of the low-level two-loop control uses an SMC with a switching surface based on the inductor current of a bidirectional converter equally for the battery and the supercapacitor, which facilitates the power decoupling and the robustness of the regulated system in the face of disturbances.

This paper is a natural continuation of the work reported in reference [14], in which the charging station was simulated in steady-state operation. It can be concluded now that all possible transitions among the different operating modes disclosed in that paper can take place automatically and can be easily regulated.

Further research will contemplate the discretization of the control system with the aim of developing a digital implementation in a reduced scale demonstrator of the hybrid microgrid. This will require the discretization of the continuous-time description of the two-loop control scheme, which will probably bring about new interesting subjects for discussion.

Author Contributions: Conceptualization, A.B.-F., D.Z.-P., O.L.-S., L.V.-S. and L.M.-S.; Methodology, A.B.-F., D.Z.-P. and L.M.-S.; Software, A.B.-F. and D.Z.-P.; Validation, A.B.-F. and D.Z.-P.; Formal analysis, A.B.-F., D.Z.-P., O.L.-S. and L.M.-S.; Investigation, L.M.-S. and A.E.A.; Supervision, D.Z.-P. and L.M.-S. All authors have read and agreed to the published version of the manuscript.

Funding: This work has been sponsored by the Spanish Ministerio de Ciencia e Innovación under grants PID 2019-111443RB-I00 and PID2020-120151RB-100 and partially supported by grant MSCA IF EF-ST 2020/PCI2021-122066-2B, financed by MCIN/AEI/10.13039/501100011033 and by the European Union NextGenerationEU/PRTR.

Data Availability Statement: Data are contained within this article.

Conflicts of Interest: The authors declare no conflicts of interest.

Abbreviations

The following abbreviations are used in this manuscript:

| | |
|-------|--------------------------------------|
| UFCS | Ultrafast charging station |
| HESS | Hybrid energy storage system |
| EVs | Electric vehicles |
| CC-CV | Constant current–constant voltage |
| ac | Alternating current |
| dc | Direct current |
| SMC | Sliding mode control |
| MV | Medium voltage |
| SST | Solid-state transformer |
| ESS | Energy storage system |
| ESD | Energy storage device |
| BESS | Battery energy storage system |
| SESS | Supercapacitor energy storage system |
| ChPs | Charging points |
| SOC | State of charge |

References

1. Ravichandran, A.; Malysz, P.; Siropour, S.; Emadi, A. The critical role of microgrids in transition to a smarter grid: A technical review. In Proceedings of the IEEE Transportation Electrification Conference and Expo: Components, Systems, and Power Electronics—From Technology to Business and Public Policy (ITEC), Metro Detroit, MI, USA, 16–19 June 2013.
2. Suarez, C.; Martinez, W. Fast and Ultra-Fast Charging for Battery Electric Vehicles—A Review. In Proceedings of the IEEE Energy Conversion Congress and Exposition (ECCE), Baltimore, MD, USA, 29 September–3 October 2019; Volume 9, pp. 569–575.
3. Srdic, S.; Lukic, S. Toward Extreme Fast Charging: Challenges and Opportunities in Directly Connecting to Medium-Voltage Line. *IEEE Electr. Mag.* **2019**, *7*, 22–31. [[CrossRef](#)]

4. Ahmad, A.; Qin, Z.; Wijekoon, T.; Bauer, P. An Overview on Medium Voltage Grid Integration of Ultra-Fast Charging Stations: Current Status and Future Trends. *IEEE Open J. Ind. Electron.* **2022**, *3*, 420–447. [[CrossRef](#)]
5. Domínguez-Navarro, J.A.; Dufo-López, R.; Yusta-Loyo, J.M.; Artal-Sevil, J.S.; Bernal-Agustín, J.L. Design of an electric vehicle fast-charging station with integration of renewable energy and storage systems. *Int. J. Electr. Power Energy Syst.* **2019**, *105*, 46–58. [[CrossRef](#)]
6. Rafi, M.A.H.; Bauman, J. A Comprehensive Review of DC Fast-Charging Stations with Energy Storage: Architectures, Power Converters, and Analysis. *IEEE Trans. Transp. Electrif.* **2021**, *7*, 345–368. [[CrossRef](#)]
7. Khalid, M.R.; Khan, I.A.; Hameed, S.; Asghar, M.S.J.; Ro, J.S. A Comprehensive Review on Structural Topologies, Power Levels, Energy Storage Systems, and Standards for Electric Vehicle Charging Stations and Their Impacts on Grid. *IEEE Access* **2021**, *9*, 128069–128094. [[CrossRef](#)]
8. Unamuno, E.; Barrena, J.A. Hybrid ac/dc microgrids—Part I: Review and classification of topologies. *Renew. Sustain. Energ. Rev.* **2015**, *52*, 1251–1259. [[CrossRef](#)]
9. Rivera, S.; Kouro, S.; Vazquez, S.; Goetz, S.M.; Lizana, R.; Romero-Cadaval, E. Electric Vehicle Charging Infrastructure: From Grid to Battery. *IEEE Ind. Electron. Mag.* **2021**, *15*, 37–51. [[CrossRef](#)]
10. Zhao, Z.; Xu, M.; Lee, C.K.M. Capacity Planning for an Electric Vehicle Charging Station Considering Fuzzy Quality of Service and Multiple Charging Options. *IEEE Trans. Veh. Technol.* **2021**, *70*, 12529–12541. [[CrossRef](#)]
11. Zambrano-Prada, D.; Lopez-Santos, O.; Martinez-Salamero, L. Dynamic power sharing strategy for hybrid energy storage system based on sliding mode control. In Proceedings of the IECON 2019—45th Annual Conference of the IEEE Industrial Electronics Society, Lisbon, Portugal, 14–17 October 2019; Volume 2019, pp. 3888–3893. [[CrossRef](#)]
12. Fan, B.; Peng, J.; Yang, Q.; Liu, W. Distributed Periodic Event-Triggered Algorithm for Current Sharing and voltage Regulation in Dc Microgrids. *IEEE Trans. Smart Grid.* **2020**, *11*, 577–589. [[CrossRef](#)]
13. Zhang, N.; Sun, Q.; Yang, L.; Li, Y. Event-triggered Distributed Hybrid Control Scheme for the Integrated Energy System. *IEEE Trans. Ind. Inform.* **2022**, *18*, 835–846. [[CrossRef](#)]
14. Blanch-Fortuna, A.; Zambrano-Prada, D.; Gállego-Casals, M.; Martinez-Salamero, L. Simulation of an Ultrafast Charging Station Operating in Steady State. *Electronics* **2023**, *12*, 4811. [[CrossRef](#)]
15. Valedsaravi, S.; El Aroudi, A.; Martinez-Salamero, L. Review of Solid-State Transformer Applications On Electric Vehicle DC Ultra-Fast Charging Station. *Energies* **2022**, *15*, 5602. [[CrossRef](#)]
16. Li, T.; Zhang, J.; Zhang, Y.; Jiang, L.; Li, B.; Yan, D.; Ma, C. An Optimal Design and Analysis of a Hybrid Power Charging Station for Electric Vehicles Considering Uncertainties. In Proceedings of the IECON 2018—44th Annual Conference of the IEEE Industrial Electronics Society, Washington, DC, USA, 21–23 October 2018; Volume 12, pp. 5147–5152. [[CrossRef](#)]
17. Jing, W.; Hung Lai, C.; Wong, S.H.W.; Wong, M.L.D. Battery-supercapacitor hybrid energy storage system in standalone DCmicrogrids: A review. *IET Renew. Power Gener.* **2017**, *11*, 461–469. [[CrossRef](#)]
18. Díaz-González, F.; Aragüés-Peñalba, M.; Girbau-Llistuella, F.; Llonch Masachs, M.; Sumper, A. A power sharing algorithm for a hybrid energy storage system based on batteries. In Proceedings of the 2019 IEEE PES Innovative Smart Grid Technologies Europe (ISGT-Europe), Bucharest, Romania, 29 September–2 October 2019. [[CrossRef](#)]
19. Meng, L.; Zafar, J.; Khadem, S.K.; Collinson, A.; Murchie, K.C.; Coffele, F.; Burt, G.M. Fast Frequency Response From Energy Storage Systems—A Review of Grid Standards, Projects and Technical Issues. *IEEE Trans. Smart Grid* **2020**, *11*, 1566–1581. [[CrossRef](#)]
20. Venkataraman, R. Sliding Mode Control of Power Converters. Ph.D. Thesis, California Institute of Technology, Pasadena, CA, USA, 6 May 1986.
21. Utkin, V.I.; Guldner, J.; Shi, J. *Sliding Mode Control in Electro-Mechanical Systems*, 2nd ed.; CRC Press: Boca Raton, FL, USA, 2009.
22. Tan, S.C.; Lai, Y.M.; Tse, C.K. General Design Issues of Sliding-Mode Controllers in DC–DC Converters. *IEEE Ind. Electron. Mag.* **2008**, *11*, 1160–1174. [[CrossRef](#)]
23. Sira-Ramírez, H.; Silva-Ortigoza, R. *Control Design Techniques in Power Electronics Devices*, 2006th ed.; Springer: Berlin/Heidelberg, Germany, 2006; pp. 61–122.

Disclaimer/Publisher’s Note: The statements, opinions and data contained in all publications are solely those of the individual author(s) and contributor(s) and not of MDPI and/or the editor(s). MDPI and/or the editor(s) disclaim responsibility for any injury to people or property resulting from any ideas, methods, instructions or products referred to in the content.